# Tracking for Maneuvering Target Trajectories via the 3D Circular Filter

**DIRK TENNE**
**TARUNRAJ SINGH**
SUNY Buffalo

**A circular prediction algorithm is proposed, which integrates the measured data into the filter and constrains the prediction to lie on a smooth curve modeled by an arc of a circle. The circular prediction is entirely defined in relation to three measurements in three-dimensional space. It is therefore not necessary to calculate the center and the radius of the circle. To obtain the statistics of the circular prediction, the unscented transformation has been utilized. The proposed hybrid filter combines the circular prediction and a constant velocity prediction by utilizing the covariance intersection (CI). This combined prediction can be updated with the subsequent measurement using a linear estimator. The proposed technique is compared with standard filters and the interacting multiple model (IMM) approach on a benchmark trajectory which includes coordinated turns and straight line maneuvers.**

Manuscript received February 17, 2004; revised November 9, 2004; released for publication April 22, 2005.

IEEE Log No. T-AES/41/4/860800.

Refereeing of this contribution was handled by B. La Scala.

Authors' addresses: D. Tenne, Center for Multisource and Information Fusion, SUNY Buffalo, Buffalo, NY; T. Singh, Dept. of Mechanical and Aerospace Engineering, SUNY Buffalo, 1009 Furnas Hall, Buffalo, NY 14260-4400, E-mail: (tsingh@eng.buffalo.edu).



## I. INTRODUCTION

The estimation and prediction of the kinematics of a dynamic object requires the use of a dynamic model and discrete time data. A majority of target trackers are based on a straight line maneuver such as $\alpha$-$\beta$ [1–3], $\alpha$-$\beta$-$\gamma$ [4, 5] and linear Kalman filters [6–8]. The model uncertainties and the pilot-induced maneuvers are accounted for as stochastic acceleration [9, 10]. Farooq et al. [11, 12] present various maneuver compensation techniques. The ambiguousness of the maneuver models has been compensated by designing algorithms consisting of multiple models [13–18]. On the contrary, complex nonlinear models have been developed to capture the real object dynamics [19–21]. These models are applied to special maneuvers such as the coordinated turn [22, 23]. In general the coordinated turn models are a set of nonlinear, coupled equations, which are difficult to solve. The focus of the work presented here is on the development of an algorithm constraining the predicted state to a circular path.

The unscented transformation developed by Julier and Uhlmann [24] is used in conjunction with the circular target motion model derived here. The key feature of the unscented transformation is that it approximates the probability distribution rather than approximating the nonlinear function by a Taylor series. A review of the development and modifications of the original unscented transformation is presented in [25]. In addition, the proposed hybrid filter utilizes the covariance intersection (CI) algorithm developed by Uhlmann [26], [27] to combine the maneuvering and nonmaneuvering modes. The CI is a conservative fusion technique if the cross-correlation is unknown. Uhlmann arrived at the CI algorithm by showing that the solution of a conservative fusion yielding a positive definite error covariance, is a function of a scalar weight $w$ only.

A geometric approach of implementing a circular turn has been introduced by Roecker and McGillem [28]. It has been observed that aircrafts normally maneuver on circular paths and a new polar coordinate system has been implemented at the center of the maneuver. Kawase et al. [29] designed an $\alpha$-$\beta$ filter in conjunction with a two-dimensional circular prediction algorithm. In [30] Kawase et al. combined the circular prediction with a two-stage Kalman filter, which has been used for maneuvering targets by Alouani et al. [8]. The center-point approach (CPA) predicts in a polar coordinate system ($R$ and $\psi$) whose origin is the center of the circle. The CPA is not amenable for further stability, performance and uncertainty analysis, because of the complex center coordinate calculation and discontinuities in the polar angle $\psi$ between successive scans. This discontinuity appears by switching from the previous circle to the next circle as the radius and center change. Moreover,

this algorithm has to distinguish between clockwise and counterclockwise turns. Tenne and Singh [31] presented a circular tracking algorithm in a local coordinate system retaining a set of states to avoid such discontinuities.

This paper develops a three-dimensional tracking algorithm for maneuvering trajectories. Section II introduces the planar circular tracking technique in a local coordinate system, which is amenable to extension to a three-dimensional tracking algorithm as proposed in Section III. This section derives the circular prediction plane on which the prediction is performed using the Unscented transformation. The Hybrid filter is introduced as a convex combination of the circular prediction and a constant velocity prediction. The paper concludes with an illustration of the proposed technique on a benchmark trajectory consisting of coordinated turns and straight line maneuvers.

## II. THE PLANAR CIRCULAR TRAJECTORY CONSTRAINT

To develop the algorithm, consider four points lying on a circle as shown in Fig. 1(a). The four points are connected to create two triangles $\triangle 123$ and $\triangle 134$, where the triangle sides are named by the points which they connect, for example, $R_{12}$ is the distance between points ① and ②. The fourth point can be described relative to the points ① to ③ by a variety of angle and distance combinations. A convenient pair is the angle $\varphi_2$ and the distance $R_{34}$ as indicated in Fig. 1(b). The desired prediction equations define the relationships between the fourth point, which is parameterized by $R_{34}$ and $\varphi_2$ and the previous three points. To derive the prediction equation, consider the points ②, ③, and ④ relative to point ①, which is equivalent to introducing a Cartesian coordinate system labeled $u$-$v$ with its origin at point ①. Observing Fig. 1(b), the distances are defined in terms of $u_i$ and $v_i$.

$$R_{13}^2 = u_3^2 + v_3^2 \tag{1a}$$

$$R_{14}^2 = u_4^2 + v_4^2 \tag{1b}$$

$$R_{24}^2 = (u_4 - u_2)^2 + (v_4 - v_2)^2 \tag{1c}$$

$$R_{34}^2 = (u_4 - u_3)^2 + (v_4 - v_3)^2. \tag{1d}$$

Equations (1c) and (1d) can be rewritten as

$$u_2u_4 + v_2v_4 = R_{12}R_{14}\cos(\varphi_1 + \varphi_2) \tag{2a}$$

$$u_3u_4 + v_3v_4 = R_{13}R_{14}\cos\varphi_2 \tag{2b}$$

and solving for the relative position $[u_4 \;\; v_4]^T$, yields the desired relationship

$$\begin{bmatrix} u_4 \\ v_4 \end{bmatrix} = \begin{bmatrix} u_2 & v_2 \\ u_3 & v_3 \end{bmatrix}^{-1} \begin{bmatrix} R_{12}\cos(\varphi_1 + \varphi_2) \\ R_{13}\cos\varphi_2 \end{bmatrix} R_{14}. \tag{3}$$

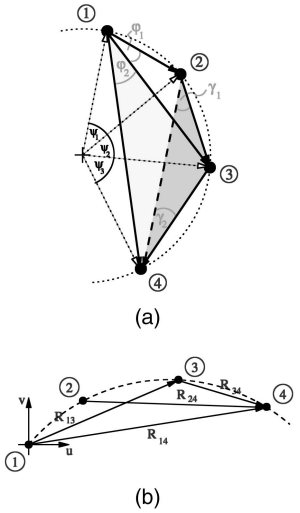


Fig. 1. Properties of points lying on a circle. (a) Basic properties. (b) Relative relationships.

The unknown distance $R_{14}$ in (3) is determined from $\triangle 134$ using the cosine rule

$$R_{14} = R_{13}\left[\cos\varphi_2 \pm \sqrt{\left(\frac{R_{34}}{R_{13}}\right)^2 - \sin^2\varphi_2}\right]. \tag{4}$$

In case of a prediction with constant angular velocity ($\varphi_2 = \varphi_1$ and $R_{34} = R_{23}$) it can be shown that the smaller value of (4) yields the trivial solution of $R_{14} = R_{12}$, and therefore the desired relationship for the prediction is the positive radical. This equation is also valid for the nonconstant angular velocity case since the smaller value of $R_{14}$ would place the predicted position in the vicinity of point ②, which is not the desirable solution.

From the triangle $\triangle 234$ in Fig. 1(a), the variable $R_{34}$ can be calculated using the sine theorem

$$R_{34} = \frac{\sin\gamma_1}{\sin\gamma_2}R_{23} = \frac{\sin\varphi_2}{\sin\varphi_1}R_{23} \tag{5}$$

where the relationships $\gamma_1 = \varphi_2$ and $\gamma_2 = \varphi_1$ have been applied, which can be easily observed from Fig. 1(a).

The solution of $R_{14}$ (4) contains the evaluation of a square root, whose radicand can take negative values and can cause numerical instability. It is therefore, desirable to derive an alternative form, which proves advantageous in the prospective development. An alternative equation for the distance $R_{14}$ can be obtained by substituting (5) into (4) and rearranging leading to

$$R_{14} = R_{13}\cos\varphi_2 + \frac{\sin\varphi_2}{\sin\varphi_1}\sqrt{R_{23}^2 - R_{13}^2\sin^2\varphi_1}. \tag{6}$$

The square root expression can be modified by observing Fig. 2, where the triangle $\triangle 123$ has been extended in the direction of the phasor $R_{12}$ to build a

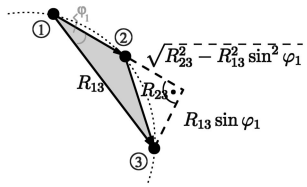


Fig. 2. Right angle triangle extension to triangle △123.

right angle triangle with the hypotenuse $R_{13}$

$$\sqrt{R_{23}^2 - R_{13}^2 \sin^2\varphi_1} = R_{13}\cos\varphi_1 - R_{12}.$$

Further simplification with the use of the sum of angle theorem leads to

$$R_{14} = [R_{13}\sin(\varphi_1 + \varphi_2) - R_{12}\sin\varphi_2]\frac{1}{\sin\varphi_1}. \quad (7)$$

Note that (7) is also valid for straight line maneuvers. Assuming a constant speed (CS) angular turn (7) reduces to

$$R_{14}^{\mathrm{CS}} = 2R_{13}\cos\varphi_2 - R_{12} \quad (8)$$

and in case of a straight line maneuver

$$\lim_{\varphi_1 \to 0} R_{14}^{\mathrm{CS}} = 2R_{13} - R_{12}. \quad (9)$$

For prospective development of a three-dimensional extension of the proposed algorithm, the prediction (3) can be interpreted as a vector quantity. Define the vector $\vec{r}_{12}$ of length $R_{12}$ pointing from point ① towards point ②, and vector $\vec{r}_{13}$, respectively. By evaluating the matrix inverse and noticing that the determinant can be expressed as $u_2 v_3 - u_3 v_2 = R_{12}R_{13}\sin\varphi_1$, which is a direct result of the cross product performed in a two-dimensional plane

$$\|\vec{r}_{13} \times \vec{r}_{12}\| = R_{12}R_{13}\sin\varphi_1 \quad (10)$$

the prediction equation (3) can be rewritten as

$$\begin{bmatrix} u_4 \\ v_4 \end{bmatrix} = T(\pi/2)\vec{n}_{13}R_{14}\frac{\cos(\varphi_1 + \varphi_2)}{\sin\varphi_1} + T(-\pi/2)\vec{n}_{12}R_{14}\frac{\cos\varphi_2}{\sin\varphi_1}. \quad (11)$$

The following substitutions have been introduced. The matrix $T(\alpha)$ is the rotational transformation matrix defined as

$$T(\alpha) = \begin{bmatrix} \cos\alpha & \sin\alpha \\ -\sin\alpha & \cos\alpha \end{bmatrix}. \quad (12)$$

The normalized vector $\vec{n}_{12}$ is the unit vector pointing in the direction of $\vec{r}_{12}$. The new prediction (11) consists of a summation of the rotated and scaled unit vectors $\vec{n}_{12}$ and $\vec{n}_{13}$ in a two-dimensional plane. In a three-dimensional environment the same rotation has to be performed around the normal vector defined by the two-dimensional plane.

## III. THE THREE DIMENSIONAL EXTENSION

Commonly target position estimators function in a three-dimensional environment. The radar measurements, for example, are obtained in a spherical coordinate system reporting the range, azimuth, and elevation, whereas the target's position is described in a global Cartesian coordinate system. Kawase et al. [32] applied his two-dimensional CPA to a three-dimensional prediction, where the prediction is performed on a turning plane and its normal vector is being estimated. The proposed curve-fitting estimator constrains the prediction to a circular trajectory in a two-dimensional coordinate system. This section addresses the fact that the three points form a two-dimensional plane, which is oriented in three-dimensions. The circular estimation can be performed in this two-dimensional plane and later back-transformed to the global three-dimensional coordinate system.

### A. Representing the Circular Prediction Plane

The circular prediction algorithm described in the previous section is performed based on three position measurements. These three locations define two vectors $\vec{r}_{12}$ and $\vec{r}_{13}$ as shown in Fig. 1, which span a two-dimensional plane in three-dimensional space. The normal vector $\vec{n}_s$ of the two-dimensional plane can be obtained by evaluating the normalized cross product between $\vec{r}_{12}$ and $\vec{r}_{13}$. The orientation of the normal vector is positive when the three vectors constitute a right-handed coordinate system, which can also be determined by the right-hand screw rule rotating $\vec{r}_{12}$ into the direction of $\vec{r}_{13}$. The transition from the original Cartesian coordinate system to the circular prediction plane can be achieved by a multi-step rotation of the coordinate system. The first step consists of a rotation around the z-axis such that the projection of the normal vector onto the x-y plane aligns with the x-axis. This rotation is performed by the three-dimensional transformation matrix $G_1(\varphi_s)$, where $\varphi_s$ is the polar rotation angle of the normal vector projected on to the x-y plane. Subsequent to the alignment with the x-axis, the second step rotates the coordinate system around the transformed y-axis. This rotation is performed by the rotation matrix $G_2(\vartheta_s)$, where $\vartheta_s$ is the direction cosine of the normal vector with respect to the z-axis. The combined coordinate transformation can be obtained by constructing the rotation matrix $G = G_2(\varphi_s)G_1(\varphi_s)$:

$$G = \begin{bmatrix} \cos\varphi_s\cos\vartheta_s & \sin\varphi_s\cos\vartheta_s & -\sin\vartheta_s \\ -\sin\varphi_s & \cos\varphi_s & 0 \\ \cos\varphi_s\sin\vartheta_s & \sin\varphi_s\sin\vartheta_s & \cos\vartheta_s \end{bmatrix}. \quad (13)$$

Note that the rotation matrices $G_i$ are orthogonal and thus $G_i^{-1} = G_i^T$.

### B. Extended Circular Prediction Algorithm

Based on the development of the two-dimensional circular prediction algorithm and the results of the circular prediction plane, this section describes the circular prediction algorithm in three-dimensional space. The fact, that the circular prediction can be described as a rotation of $\vec{r}_{12}$ and $\vec{r}_{13}$ can be exploited to extend the algorithm to include the third dimension. Equation (11) can be rewritten to include a zero z-component of the predicted position and the normalized vectors, where the rotation matrix $T(\alpha)$ can be defined as

$$T(\alpha) = \begin{bmatrix} \cos\alpha & \sin\alpha & 0 \\ -\sin\alpha & \cos\alpha & 0 \\ 0 & 0 & 1 \end{bmatrix}. \tag{14}$$

Substituting the normalized vectors $\vec{n}_{12}$ and $\vec{n}_{13}$ with vectors described in the relative Cartesian coordinates denoted by a prime (11) can be written as

$$\begin{bmatrix} u_4 \\ v_4 \\ 0 \end{bmatrix} = T(\pi/2)G \begin{bmatrix} u_3' \\ v_3' \\ w_3' \end{bmatrix} \frac{R_{14}}{R_{13}} \frac{\cos(\varphi_1 + \varphi_2)}{\sin\varphi_1} + T(-\pi/2)G \begin{bmatrix} u_2' \\ v_2' \\ w_2' \end{bmatrix} \frac{R_{14}}{R_{12}} \frac{\cos\varphi_2}{\sin\varphi_1} \tag{15}$$

where $G$ is given by (13). The circular prediction of (15) is described with respect to a Cartesian coordinate system where the x-y plane coincides with the circular prediction plane. Including the back transformation into (15) involves the evaluation of the matrix product $\mathcal{G} = G^{-1}T(\pi/2)G$. Note, since $T(-\pi/2) = T^T(\pi/2)$ and $G$ is orthogonal it can be shown that the combined transformation matrix $G^{-1}T(-\pi/2)G = \mathcal{G}^T$. Therefore, the circular prediction performed on the two-dimensional plane can be written with respect to the global Cartesian coordinate system. By adding the coordinates of the first point and substituting the relative coordinates with the global coordinates we obtain the circular prediction in global Cartesian coordinates

$$\begin{bmatrix} x_4 \\ y_4 \\ z_4 \end{bmatrix} = \mathcal{G} \begin{bmatrix} x_3 \\ y_3 \\ z_3 \end{bmatrix} s_1 + \mathcal{G}^T \begin{bmatrix} x_2 \\ y_2 \\ z_2 \end{bmatrix} s_2 + (I - \mathcal{G}s_1 - \mathcal{G}^T s_2) \begin{bmatrix} x_1 \\ y_1 \\ z_1 \end{bmatrix} \tag{16}$$

where the abbreviations:

$$s_1 = \frac{R_{14}}{R_{13}} \frac{\cos(\varphi_1 + \varphi_2)}{\sin\varphi_1}, \qquad s_2 = \frac{R_{14}}{R_{12}} \frac{\cos\varphi_2}{\sin\varphi_1} \tag{17}$$

have been introduced. Performing the circular prediction with (16), we obtain a position on the two-dimensional plane, which is furthermore constrained to lie on a circle defined by the three measurements.

## IV. DEVELOPMENT OF THE HYBRID FILTER

The unscented transformation [24] is used in conjunction with the circular target motion models as discussed in the previous section. In the following text, we describe the unscented transformation to obtain the circular prediction and its covariance, which is used in conjunction with the minimum mean square error estimator to update the prediction with the measurement.

The circular prediction on the three-dimensional prediction plane is described by (16), which depends on the three position measurements. These are generally obtained by a radar in spherical coordinates. To obtain the statistics of the circular prediction, the three measurements are stacked to form an augmented vector of length $n = 9$:

$$\mathbf{x} = [r_1 \quad \psi_{r1} \quad \vartheta_{r1} \quad r_2 \quad \psi_{r2} \quad \vartheta_{r2} \quad r_3 \quad \psi_{r3} \quad \vartheta_{r3}]^T \tag{18}$$

consisting of the radar reports as range $r$, azimuth $\psi_r$, and elevation $\vartheta_r$. Its covariance $P_x$ is a diagonal matrix with the repeated elements of the individual covariances $\sigma_r^2$, $\sigma_\psi^2$, and $\sigma_\vartheta^2$. The unscented transformation can be applied to the augmented space, where the so-called $\sigma$ points are transformed to the Cartesian coordinate system and further propagated with the circular prediction (16). The unscented transformation selects a $\sigma$-set consisting of $2n + 1$ points, which is the perturbation from the mean by a scaled deviation. The deviations $\sigma_i$ are defined as the columns of the matrix square root of $P_x$ [24], and the $\sigma$-set is defined as

$$\zeta_0 = \bar{\mathbf{x}} \tag{19}$$

$$\zeta_i = \zeta_0 + \sqrt{(n + \kappa)}\sigma_i \qquad \text{for} \quad i = 1 \ldots 2n \tag{20}$$

such that the $\sigma$-set exhibits the same probabilistic characteristics as the random variable $\mathbf{x}$ and $\kappa$ is a free variable of the unscented filter, which in this particular application has been set to 2. The weights $w_0 = \kappa/(n + \kappa)$ and $w_i = 1/(2(n + \kappa))$ have been selected to match the first four central moments of $\mathbf{x}$, which is true for all Gaussian random variables if $\kappa$ is selected to satisfy the constraint, $n + \kappa = 3$.

The $\sigma$-set is transformed to the Cartesian coordinate system and further propagated by the circular prediction (16). This output set labeled $\eta_i$ yields the statistics of the circular prediction (CP) (mean $x_{\text{CP}}$ and covariance $P_{\text{CP}}$) by applying

$$x_{\text{CP}} = \bar{\eta} = \sum_{i=0}^{2n} w_i \eta_i \tag{21}$$

$$P_{\text{CP}} = P_\eta = \sum_{i=0}^{2n} w_i (\eta_i - \bar{\eta})(\eta_i - \bar{\eta})^T. \tag{22}$$

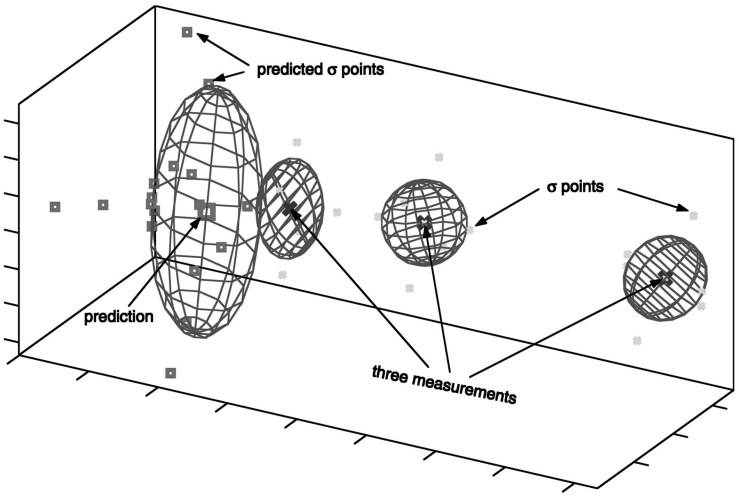


Fig. 3. Unscented $\sigma$-set illustrated on the circular prediction.

Fig. 3 illustrates the $\sigma$-set and the propagation on an example configuration. The position uncertainties are symbolized by the 1-$\sigma$ covariance ellipsoids. The standard unscented transformation creates 19 circular trajectories, i.e., 19 possible combinations of the three uncertain measurements, to determine the statistics of the circular prediction. The small squares indicate these predictions, which result in the mean and covariance by evaluating the weighted sum. The mean and covariance are illustrated by the large square and the prediction ellipsoid.

The predicted mean and covariances can now be used in the minimum mean square error estimator to update the prediction with the measurement, which has been converted to the Cartesian coordinates using an unbiased transformation [33].

### A. The Hybrid Filter

The prediction algorithms constraining the target motion on a smooth curve provide a reasonable performance for circle-like trajectories. However, real target motions can be approximated by piecewise curves which are circles and straight lines. Furthermore, with the presence of noise, the performance of a stand-alone circular filter would degrade. The proposed circular filter is therefore integrated with traditional filters including straight line target models.

The constant velocity model in three-dimensions includes the x, y, z position as well as the three velocities $v_x$, $v_y$, and $v_z$, such that the state transition matrix can be constructed as shown in Appendix A. This system is driven by white noise accelerations separated in each direction, and the process noise covariance can be calculated as shown in Appendix A, where the inverse three-dimensional rotation matrix of (13) has to be utilized. The radar measurements are obtained in the spherical coordinate system reporting the range ($r$), azimuth ($\psi$), and elevation ($\vartheta$), which are related to the Cartesian coordinate system centered at the radar location by the standard spherical to Cartesian coordinate transformation. With the aforementioned derivations it is of relative ease to program the extended Kalman filter algorithm.

The hybrid filter consists of a convex combination of the circular prediction and the predicted position of the extended Kalman filter. These predictions are statistically correlated since they are conditioned on the same measurements. Therefore, the fusion is performed using the CI algorithm developed by Uhlmann [34]. In contrast to the Kalman filter update, the CI does not assume independent data to be fused, thus yielding a conservative fusing algorithm. Assume two random processes A and B, which are described by their means (a, b) and covariances ($P_a$,$P_b$). The fused mean and covariance can be obtained as

$$P_c^{-1} = wP_a^{-1} + (1-w)P_b^{-1} \tag{23}$$

$$P_c^{-1}\mathbf{c} = wP_a^{-1}\mathbf{a} + (1-w)P_b^{-1}\mathbf{b} \tag{24}$$

where $w$ takes values in the range of $[0,1]$. The weight $w$ can be interpreted as a tuning parameter of the CI. Its selection shapes the estimated covariance either closer to the covariance of $A$ ($w \to 1$) or to the covariance of $B$ ($w \to 0$). In the following section, both random processes are equally weighted ($w = 0.5$). Upon arrival of a new measurement, the combined prediction can be updated using the linear estimator.

## V. BENCHMARK TRAJECTORY IN THREE DIMENSIONS

This section presents the performance characteristics of the proposed hybrid filter compared with the extended Kalman filter with a straight line constant velocity model and the interacting multiple model (IMM) algorithm with the modes described in the subsequent text. The benchmark

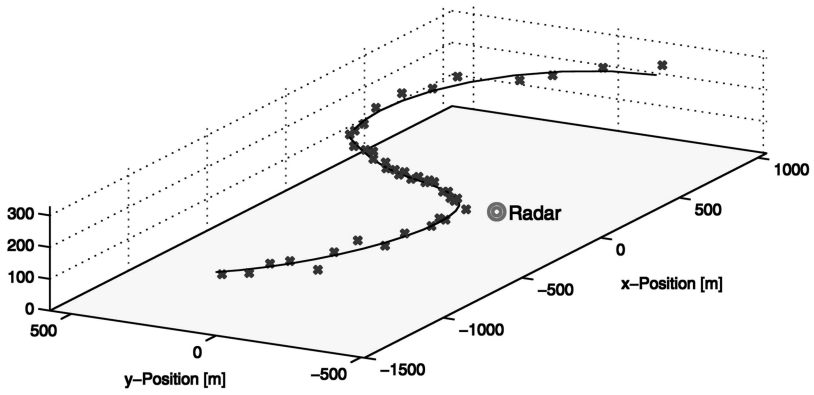


Fig. 4. Benchmark target maneuver with sample measurements.

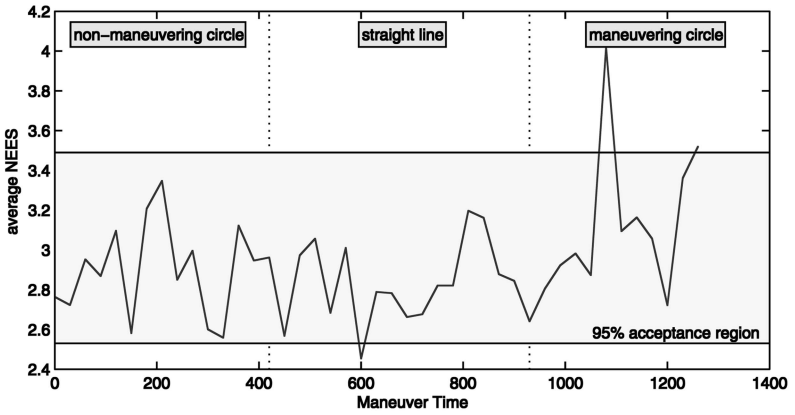


Fig. 5. Consistency test of hybrid three-dimensional filter.

trajectory facilitates a combination of coordinated turns and straight line maneuvers with constant, zero, and increasing acceleration phases. The benchmark considers a target whose position is sampled every $T = 30$ s as shown in Fig. 4. A sample of measurements is indicated by the markers $\times$. The target maneuver consists of three parts in the x-y plane:

1) a circular trajectory with constant angular velocity, resulting in a constant acceleration of 0.0132 m/s$^2$,

2) a straight line maneuver with constant speed,

3) an accelerating target on a circular trajectory, resulting in an increasing acceleration up to 0.053 m/s$^2$,

where the target speed lies in the range of 2.62 m/s–5.56 m/s. The targets elevation is simulated as an up-and-down maneuver comparable to a sine function. The targets position is reported by a stationary radar located at the x = −250 m, y = 200 m and z = 0 m as indicated by the circled position. The measurements are obtained in the radar coordinate system as range bearing whose standard deviation in range is 10 m and 2 deg in the bearing angles.

All filters have been initialized with the first three measurements and when necessary the velocity state has been evaluated from the finite difference, whereas the initial position covariance is the measurement covariance $R_k$ at time $k$ converted into Cartesian coordinates $R_k^c$. The velocity state covariance is initialized as $(R_2^c + R_3^c)/T^2$ due to the finite difference.

A consistency test as described in [35] has been carried out to ensure proper operation of the hybrid filter. A filter is called consistent if its state estimation is unbiased and the error covariance is correctly approximated by the filter's state covariance matrix. This test is performed off-line as Monte Carlo simulation, where the ground truth is known. The hypothesis $H_0$ postulates that the normalized estimation error squared equals the dimension of the state. Performing a Monte Carlo simulation the hypothesis $H_0$ can be accepted if the test statistic lies in the two-sided 95% probability concentration region. Fig. 5 shows this region along with the average normalized estimation error squared (NEES) based on 100 Monte Carlo runs. Only a small part lies outside the 95% region and the $H_0$ hypothesis can be accepted. Note that most filters fail to be consistent during maneuvers that are outside of their respective models.

A statistical comparison of the filters can be achieved by a simple hypothesis test [35, pp. 76–77]. Define the performance measure as the absolute

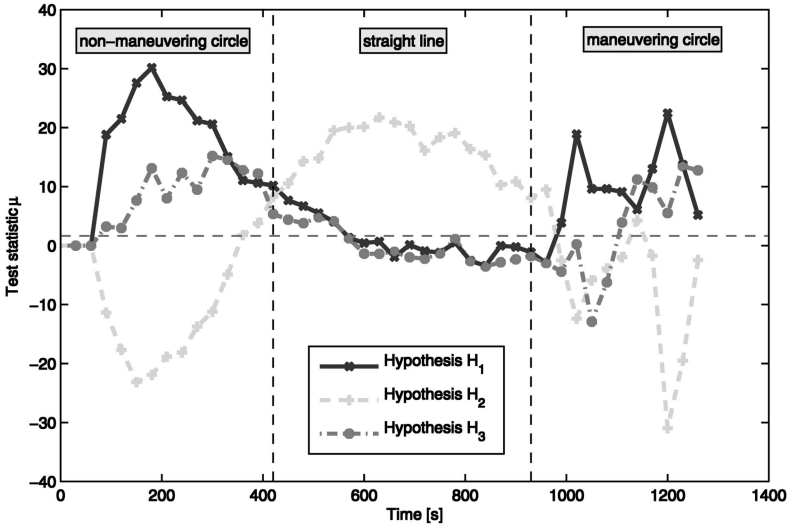


Fig. 6. Statistical test comparison of hypotheses $H_1$ and $H_2$.

estimation error $\epsilon_{\text{filter}}(k)$. Let us postulate the hypothesis that the error of filter 1 is larger than the error of filter 2:

$$H_1: \quad \Delta(k) = \epsilon_{\text{filter1}}(k) - \epsilon_{\text{filter2}}(k) > 0. \tag{25}$$

Based on Monte Carlo simulations the test statistic

$$\mu(k) = \frac{\bar{\Delta}(k)}{\sigma_{\Delta}(k)} \tag{26}$$

can be calculated, where the $\bar{\Delta}$ corresponds to the mean of $\Delta(k)$ and $\sigma_{\Delta}(k)$ represents the deviation. If $\mu$ exceeds a threshold $\mu_0$ then the hypothesis $H_1$ is accepted. The threshold is commonly defined by the significance level of the null hypothesis.

The statistical test is performed to compare the performance of the straight line (SL) model to the combined straight line and circular prediction (hybrid) model. The hypothesis is postulated as

$$H_1: \quad \Delta(k) = \epsilon_{\text{SL}}(k) - \epsilon_{\text{hybrid}}(k) > 0. \tag{27}$$

The second hypothesis $H_2$ compares the circular filter with the hybrid filter. Both test statistics are shown in Fig. 6. The hypothesis $H_1$ compares the hybrid filter with the extended Kalman filter using a straight line model, and it can be observed that the hybrid filter performs better during the circular maneuver since the test statistic is above the threshold, whereas during the straight line maneuver the test statistic falls below the threshold. The comparison of the circular filter and the hybrid filter yields better performance for the circular filter during the turning maneuvers and the hybrid filter exhibits increased performance during the straight line maneuver.

The third test $H_3$ compares the IMM algorithm with the proposed hybrid filter. The three-mode IMM consists of a constant velocity model and a Wiener process acceleration model with two process noise settings $q_2 = 0.0132^2$ and $q_3 = 0.0331^2$, which correspond to the minimum acceleration and the average acceleration. The Markov chain transition matrix between these models

$$p_{ij} = \begin{bmatrix} 0.9 & 0.09 & 0.01 \\ 0.15 & 0.7 & 0.15 \\ 0.01 & 0.15 & 0.84 \end{bmatrix} \tag{28}$$

has been chosen to indicate a strong likelihood to operate at the current model and to allow a smooth transition between the constant velocity and slow accelerating and fast accelerating models. Fig. 6 shows the result of the statistical comparison as defined by (26). The hybrid filter outperforms the IMM algorithm during the constant acceleration phase, whereas the IMM yields a better performance during the constant velocity phase. As the acceleration is increasing both filters perform well. The transition of the IMM to the acceleration phase appears faster than the one of the hybrid filter, which exhibits a smaller error at the mid-phase of the maneuvering circle path. Fig. 7 compares the combined position rms error of the proposed hybrid and the IMM algorithm. Throughout the benchmark trajectory both filters perform likewise, whereas the IMM algorithm exhibits a lower rms error during the constant velocity path and during the transition to the turning phase. The initial peak of the IMM is the result of the finite difference velocity initialization.

## VI. REMARKS AND CONCLUSION

In real applications the filters are confronted with missed and false measurements. In case of missing measurements the proposed filter remains predicting on the previous circular path until a new measurement arrives. The missed measurements subsequently

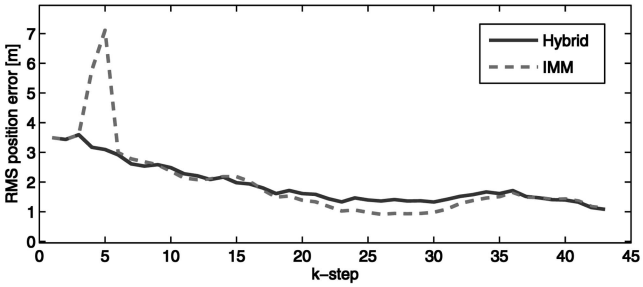


Fig. 7. Combined position rms error comparison.

have to be replaced by the corresponding prediction. The limits on how long this filter can predict on the previous circle and when the target is declared to be lost have to be identified. False radar reports could be handled by the circular filter using a least squares approach to identify the circular path based on the history of a window of measurements.

In this work, the fact that a target trajectory has to be smooth even if the acceleration is impulsive has been exploited to develop a new technique for target tracking. The proposed algorithm integrates the measured data into the filter and constrains the prediction to lie on a smooth curve, modeled, for example by the arc of a circle. This filter recalculates the equations of the circle at every time instant and thus, in the presence of reasonably fast sampling approximates any smooth trajectory via multiple arcs of circles.

The development of the circular filter is illustrated in two-dimensional space and subsequently extended to three-dimensional space using orthogonal transformations. For the determination of the covariance of the estimate, the proposed algorithm relies on the unscented transformation, a novel approach to approximate the statistics of a random variable subject to a nonlinear transformation. The use of the unscented transformation enables us to calculate the statistics of the circular prediction algorithm.

The hybrid filter consists of a combination of the straight line prediction and the circular prediction. It has been shown on a benchmark maneuver that the hybrid filter outperforms standard filters, such as the extended Kalman filter using a straight line model. In addition, a closed-form solution to the circular prediction algorithm has been derived, which has been implemented in conjunction with the extended Kalman filter. Statistical tests have been performed to validate the performance increase using the hybrid filter.

The proposed filter in two-dimensional or three-dimensional can complement the bank of filters in an IMM filter [35] or the variable-dimension filter developed by Bar-Shalom and Birmiwal [14]. Maneuver detectors have been applied to switch between different target models describing various maneuvers of the target.

## APPENDIX A. CONSTANT VELOCITY MODEL

A common model used for target tracking, assumes a target moving on a straight line with a constant velocity, where the system is driven by white noise acceleration. The linear state space is comprised of the Cartesian position and its corresponding velocities yielding the state transition matrix:

$$\Phi = \begin{bmatrix} \mathbf{I}^{n\times n} & T\mathbf{I}^{n\times n} \\ 0^{n\times n} & \mathbf{I}^{n\times n} \end{bmatrix} \tag{29}$$

where $\mathbf{I}^{n\times n}$ is the identity matrix of dimension $n = 3$ and $0^{n\times n}$ corresponds to the null matrix. The measurements are again assumed to be the radar reports in polar coordinates. Subsequently, the extended Kalman filter equations have to be applied. This model is driven by white noise acceleration, which can be best described in the target's coordinate frame, where the Cartesian abscissa is aligned with the heading direction. The accelerations are divided into the parallel acceleration $a_p$, the normal acceleration $a_n$ acting on the target in perpendicular direction, and the binormal acceleration $a_b$. The variances are defined as $\sigma_p^2$, $\sigma_n^2$, and $\sigma_b^2$, respectively. The covariance matrix described in the Cartesian system can be obtained using the inverse three-dimensional rotation matrix of (13)

$$S_{\text{cart}} = G^T \text{diag}[\sigma_p^2 \quad \sigma_n^2 \quad \sigma_b^2]G. \tag{30}$$

The process noise $Q_d$ is recalculated for every time step. Due to the nonlinear state space system, the orientation of the covariances depends on the heading angle $\vartheta$. Assuming a discretized white noise the process noise is defined as [6]:

$$Q_d = E\left\{\int_0^T \int_0^T \Phi(T-\tau_1)Bw_c(\tau_1)w(\tau_2)_c^T B^T \Phi(T-\tau_2)^T d\tau_1 d\tau_2\right\} \tag{31}$$

where $\Phi$ is the Jacobian of the state space, $B$ is the input matrix, and $w_c$ is the continuous white noise vector with the covariance $E\{w_c(\tau_1)w(\tau_2)_c^T\} = Q_c\delta(\tau_2 - \tau_1)$

$$Q_d = \begin{bmatrix} \frac{T^3}{3}S_{\text{cart}} & \frac{T^2}{2}S_{\text{cart}} \\ \frac{T^2}{2}S_{\text{cart}} & TS_{\text{cart}} \end{bmatrix}. \tag{32}$$

REFERENCES


[1] Sklansky, J.
Optimizing the dynamic parameter of a track-while-scan system.
RCA Laboratories, Princton, NJ, June 1957.

[2] Benedict, T. R., and Bordner, G. W.
Synthesis of an optimal set of radar track-while-scan smoothing equations.
*IRE Transactions on Automatic Control*, **AC-1** (July 1962).

[3] Kalata, P. R.
$\alpha - \beta$ target tracking systems: A survey.
In *Proceedings of the American Control Conference*, 1992.

[4] Simpson, H. R.
Performance measures and optimization condition for a third order sampled-data tracker.
*IEEE Transactions on Automatic Control*, **AC-12** (June 1962).

[5] Kalata, P. R.
The tracking index: A generalized parameter for $\alpha - \beta$ and $\alpha - \beta - \gamma$ target trackers.
*IEEE Transactions on Aerospace and Electronic Systems*, **AES-20**, 2 (Mar. 1984).

[6] Bar-Shalom, Y., and Fortmann, T. E.
*Tracking and Data Association*.
New York: Academic Press, 1988.

[7] Lawton, J. A., Jesionowski, R. J., and Zarchan, P.
Comparison of four filtering options for radar tracking problem.
*Journal of Guidance, Control and Dynamics*, **21**, 4 (July 1998).

[8] Alouani, A., Xia, P., Rice, T., and Blair, W.
A two-stage Kalman estimator for tracking maneuvering targets.
In *Proceedings of the IEEE International Conference on Systems, Man, and Cybernetics*, vol. 2, 1991.

[9] Singer, R. A.
Estimating optimal tracking filter performance for manned maneuvering targets.
*IEEE Transactions on Aerospace and Electronic Systems*, **AES-5** (Nov. 1970).

[10] Berg, R. F.
Estimation and prediction for maneuvering target trajectories.
*IEEE Transactions on Automatic Control*, **AC-28** (Mar. 1983), 294–304.

[11] Farooq, M., and Bruder, S.
Information type filters for tracking a maneuvering target.
*IEEE Transactions on Aerospace and Electronic Systems*, **26**, 3 (May 1990), 441–454.

[12] Farooq, M., Bruder, S., Quach, T., and Lim, S.
Adaptive filtering techniques for manoeuvering targets.
In *Proceedings of the 34th Midwest Symposium on Circuits and Systems*, vol. 1, May 1991, 31–34.

[13] Magill, D.
Optimal adaptive estimation of sampled stochastic processes.
*IEEE Transactions on Automatic Control*, **AC-10** (1965), 434–439.

[14] Bar-Shalom, Y., and Birmiwal, K.
Variable dimension filter for maneuvering target tracking.
*IEEE Transactions on Aerospace and Electronic Systems*, **AES-18**, 5 (Sept. 1982), 621–629.

[15] Blom, H., and Bar-Shalom, Y.
The intercating multiple model algorithm for systems with markovian switching coefficients.
*IEEE Transactions on Automatic Control*, **33** (Aug. 1988), 780–783.

[16] Bar-Shalom, Y., Chang, K., and Blom, H.
Tracking a maneuvering target using input estimation vs. the interacting multiple model algorithm.
*IEEE Transactions on Aerospace and Electronic Systems*, **25** (Mar. 1989), 296–300.

[17] Jilkov, V., Angelova, D., and Semerdjiev, T.
Design and comparison of mode-set adaptive IMM algorithms for maneuvering target tracking.
*IEEE Transactions on Aerospace and Electronic Systems*, **35**, 1 (Jan. 1999), 343–350.

[18] Kirubarajan, T., and Bar-Shalom, Y.
Kalman filter versus imm estimator: When do we need the latter?
*IEEE Transactions on Aerospace and Electronic Systems*, **39**, 4 (Oct. 2003), 1452–1457.

[19] Bishop, R., and Antoulas, A. C.
Non-linear approach to the aircraft tracking problem.
*Journal of Guidance, Control and Dynamics*, **17**, 5 (Sept. 1994), 1124–1130.

[20] Blackman, S., and Popoli, R.
*Design Analysis of Modern Tracking Systems*.
Norwood, MA: Artech House, 1999.

[21] Bullock, T., and Sangsuk-Iam, S.
Maneuver detection and tracking with a nonlinear target model.
In *Proceedings of the Conference on Decision and Control*, vol. 1, Las Vegas, NV, Dec. 1984, 1122–1126.

[22] von Mises, R.
*Theory of Flight*.
New York: McGraw-Hill, 1945.

[23] Nabaa, N., and Bishop, R. H.
Validation and comparison of coordinated turn aircraft maneuver models.
*IEEE Transactions on Aerospace and Electronic Systems*, **36** (Jan. 2000), 250–259.

[24] Julier, S. J., Uhlmann, J. K., and Durrant-Whyte, H. F.
New approach for filtering nonlinear systems.
In *Proceedings of the American Control Conference*, vol. 3, 1995, 1628–1632.

[25] Julier, S., and Uhlmann, J.
Unscented filtering and nonlinear estimation.
*Proceedings of the IEEE*, **92**, 3 (Mar. 2004), 401–422.

[26] Uhlmann, J. K.
Dynamic map building and localization: New theoretical foundations.
Ph.D. dissertation, University of Oxford, Trinity Term 1995.

[27] Uhlmann, J.
Covariance consistency methods for fault-tolerant distributed data fusion.
*Information Fusion*, **4** (2003), 201–215.

[28] Roecker, J. A., and McGillem, C. D.
Target tracking in maneuver-centered coordinates.
*IEEE Transactions on Aerospace and Electronic Systems*, **25**, 6 (Nov. 1989), 836–843.

[29] Kawase, T., Tsarunosono, H., Ehara, N., and Sasase, I.
An adaptive-gain alpha-beta tracker combined with circular prediction for maneuvering target tracking.
In *Proceedings of IEEE Speech and Image Technologies For Computing and Telecommunications*, vol. 2, 1997.

[30] Kawase, T., Tsarunosono, H., Ehara, N., and Sasase, I.
Two-stage Kalman estimator using advanced circular predictions for maneuvering target tracking.
In *Proceedings of the IEEE International Conference on Acoustics, Speech, and Signal Processing*, vol. 4, May 1998.

[31] Tenne, D., and Singh, T.
Circular prediction algorithms—Hybrid filters.
In *Proceedings of the American Control Conference*, vol. 1, May 2002, 172–177.

[32] Kawase, T., Tsarunosono, H., Ehara, N., and Sasase, I.
An adaptive-gain alpha-beta tracker combined with three-dimensional circular prediction using estimation of the plane state.
In *Proceedings of the IEEE International Conference on Acoustics, Speech, and Signal Processing*, vol. 5, May 1999.

[33] Lerro, D., and Bar-Shalom, Y.
Tracking with debiased consistent converted measurements versus EKF.
*IEEE Transactions on Aerospace and Electronic Systems*, **29**, 3 (July 1993).

[34] Uhlmann, J., Julier, S., Kamgar-Parsi, B., Lanzagorta, M., and Shyu, H-J.
NASA Mars Rover: A testbed for evaluating applications of covariance intersection.
In *Proceedings of the 1999 Unmanned Ground Vehicle Technology Conference*, vol. 3693, Naval Research Lab., Washington, D.C. Also in *Proceedings of SPIE*, 1999, 140–149.

[35] Bar-Shalom, Y., and Li, X-R.
*Estimation and Tracking: Principles, Techniques and Software*.
Storrs, CT: YBS Publishing, 1998.

**Dirk Tenne** received his M.S. and Ph.D. degrees from the Department of Mechanical and Aerospace Engineering, State University of New York at Buffalo in 1998 and 2004, respectively. He received the Diplom-Ingenieur from the Technische Universität Darmstadt, Germany in 1999.

Since 2004 he is a postdoctoral fellow at the Center for Multisource and Information Fusion, SUNY Buffalo. His research includes target tracking and statistically robust controller design.

Dr. Tenne has published papers at the Fusion Conference, the American Control Conference, and the American Institute of Aeronautics and Astronautics journals.

**Tarunraj Singh** received his B.E, M.E, and Ph.D degrees in mechanical engineering from Bangalore University, Indian Institute of Science, and the University of Waterloo, respectively.

He was a postdoctoral fellow in the Aerospace Engineering Dept. of Texas A & M University prior to starting his tenure at the University at Buffalo in 1993, where he is currently a Professor in the Department of Mechanical and Aerospace Engineering. He was a von Humboldt fellow and spent his sabbatical at the Technische Universität Darmstadt in Germany and at the IBM Almaden Research center in 2000–2001. He was a NASA Summer Faculty Fellow at the Goddard Space Flight Center in 2003. His research is supported by the National Science Foundation, AFOSR, NSA, Office of Naval Research and various industries including MOOG Inc. Praxair and Delphi Thermal Systems. His research interests are in robust vibration control, optimal control, nonlinear estimation and intelligent transportation.

Dr. Singh has published over 100 refereed journal and conference papers and has presented over 30 invited seminars at various universities and research laboratories.